Thin-Walled Structures 182 (2023) 110206

Contents lists available at ScienceDirect

Thin-Walled Structures

journal homepage: www.elsevier.com/locate/tws

Full length article

Buckling resistance of a metal column in a corrugated sheet silo-experiments and non-linear stability calculations

K. Rejowski, P. Iwicki, J. Tejchman *, M. Wójcik

Gdańsk University of Technology, Poland

ARTICLE INFO

Keywords:
Metal column
Silo
Corrugated wall
Buckling resistance
FEM
Eurocode 3

ABSTRACT

The results of experimental and numerical tests of a single corrugated sheet silo column's buckling resistance are presented in this study. The experiments were performed in a real silo with and without bulk solid (wheat). A very positive impact of the bulk solid on the column buckling resistance occurred. The experimental results were first compared to the buckling resistance calculated by Eurocode 3 formulae. The comparison revealed that code formulae were overly conservative for the empty and pre-filled silo. The experiments were next simulated using the finite element method (FEM) with initial geometric imperfections, based on geodetic measurements or linear bifurcation analyses. The bulk solid's behaviour was described by two different linear elastic approaches. For real geometric imperfections, the FE computations and experimental findings were in good agreement (particularly for an empty silo). For the pre-filled silo with the code elasticity of the bulk solid and the geodetic amplitude of geometric imperfection of the empty silo, the numerical buckling resistance was too low as compared to the experimental outcomes. In addition, the model tests were performed for a single column with a corrugated sheet at the laboratory scale.

1. Introduction

Silos are engineering structures used in industries and farms to store, feed, and process bulk solids. They are utilized in agricultural, mining, mineral processing, chemical, and shipping industries, among others [1–4]. Bulk solids are frequently stored in metal cylindrical silos. Because of a compressive vertical force induced by bulk material friction on silo walls, these structures are prone to stability failure [5–8]. The loss of silo stability most frequently occurs during asymmetric filling and emptying, which is caused by the heterogeneous character of bulk solids [9,10].

To reduce material use, the walls of metal silos are made of corrugated sheets strengthened around the perimeter of silos with columns of the same spacing, connected to sheets with bolts. The corrugated sheets transmit the horizontal tensile forces from the bulk material pressure to the silo walls, and the columns transfer the vertical compressive forces from the bulk material friction against the walls [11]. According to Eurocode [12] and the amendments [13], the design criteria, based on the stability theory of the orthotropic shell or the theory of stability of a column on the elastic ground depend on the spacing of vertical columns arranged along the silo perimeter. Determining the buckling resistance of silos using the finite element method based on nonlinear static analyses of the equilibrium path between load and displacement requires complex 3D silo models, a very huge number of finite elements, and hence a long calculation time.

The simplified relationships for evaluating the standard buckling resistance of silos given in [12,13] are conservative, as they do not take into account the actual spatial strength of entire silo structures. The findings of buckling calculations using the finite element method (FEM) in [14–22] and the results of experimental studies in [23] revealed that the solutions using the Eurocode approach differed significantly from FE solutions. The noticeable underestimation of the buckling resistance of silo structures was observed for a high separation of vertical columns. The disadvantage of the approach in [12] was also the lack of continuity of the solution between the two Eurocode approaches in terms of the spacing of columns [15,16,20]. The papers [16,20,21,24] and [25] proposed changes to standard procedures, based on comprehensive numerical FE analyses of silos. The research [25] proposed e.g. a new formula for calculating the stiffness of the elastic foundation supporting the vertical silo column in the form of a corrugated sheet, which took into consideration the curvature of the cylindrical silo mantle. The formula significantly improved the standard results of the buckling resistance as compared to FEM [16]. However, the underestimation of buckling resistance of silo structures still occurred since the length of the buckling half-wave in the circumferential direction assumed in Eurocode was still too large. This solution was comparable to that in the amendment introduced to Eurocode 3 [13]. The paper [15] suggested a simplified silo model in the form of a silo segment containing 3 or 4 columns with appropriate boundary conditions along the vertical

* Corresponding author.
E-mail addresses: karrejow@pg.edu.pl (K. Rejowski), piwicki@pg.edu.pl (P. Iwicki), tejchmk@pg.edu.pl (J. Tejchman), mwojcik@pg.edu.pl (M. Wójcik).

https://doi.org/10.1016/j.tws.2022.110206
Received 28 May 2022; Received in revised form 28 August 2022; Accepted 27 September 2022
Available online xxxx

edges, allowing for the buckling resistance similar to FE results for entire silos. The effect of different wave geometry of corrugated sheets was numerically investigated in [20]. The silos with the narrow wall corrugation and high corrugation amplitude had a buckling resistance higher by 50%–100% than with the wide corrugation and low corrugation amplitude [20]. A positive effect of different vertical and horizontal corrugation-shaped stiffeners on the strength of thin-walled cylindrical shell models under external pressure was experimentally found in [26,27].

The current article presents the results of experiments and FEM calculations for the buckling of a single silo column on a laboratory scale and in a real silo. The laboratory tests were performed with a single column with and without a corrugated sheet. Column buckling experiments in a real silo were carried out for an empty silo and a pre-filled silo with wheat. First, the experimental results were compared with the Eurocode results [12,13]. Next, the experimental results on a laboratory and natural scale were simulated with non-linear stability FE calculations, where initial geometric imperfections were taken into account based on geodetic measurements of the empty silo or linear bifurcation analysis (LBA). FE analyses of a real silo additionally took into account the presence of the bulk solid, using two different linear elastic models, i.e. Winkler–Pasternak foundation and continuum solid material. The numerical results showed satisfactory agreement in comparison with the experiments, particularly for an empty silo. The numerical and experimental results in a real silo differed from those in Eurocode [12,13].

Innovative elements in our research are: (1) experimental results for a single column in a corrugated steel silo at the natural scale versus numerical non-linear stability outcomes (scientific literature lacks similar experimental results) and (2) inclusion of the bulk solid in FE analyses, which rarely take into account the positive effect of bulk solid stiffness on silo buckling resistance.

2. Experimental stands

2.1. Single column with corrugated sheet on laboratory scale

The goal of the lab tests was to evaluate the buckling resistance of a single column with a corrugated sheet as compared to a column without a corrugated sheet under the effect of a concentrated force. The lab test included two spans of the silo mantle with a total width of 1600 mm (with a column spacing of 800 mm) and a height of 1588 mm (Figs. 1 and 2). The radius of curvature of the corrugated sheet was R = 6240 mm. The base of this test stand-up was a steel frame freely resting on a rigid base, consisting of C-profiles with a cross-section height of 150 mm and a wall thickness of 4 mm "a" (Fig. 1). The frame constituted support for the outermost edges of the corrugated sheet "b" (Fig. 1). The connection of the corrugated sheet with the steel frame was made by using M10 bolts with a spacing of 76 mm along the entire length of the outer sheet edge (as in real silos). The examined steel column "c" (Fig. 1) was made of a steel flat bar with a cross-section of 50 × 6 mm^2. The cross-section of the column had low bending stiffness compared to the bending stiffness commonly used in corrugated sheet silos columns to buckle it under a relatively low load. The column was connected to the corrugated sheet along its entire length with M10 screw connectors at a spacing of 76 mm. The compressive force was introduced by hand into the flat bar by using the M16 threaded steel tie-rod "d" attached to the outermost profiles "g" (Fig. 1), connected to the flat bar at its ends. The outermost nodes "f" (Fig. 1) provided rigid support for the compressed flat bar, allowing free displacement along the action of loads. To limit the rotations of outermost nodes, an additional stiffening C-profile "e" was used (Fig. 1). The compressed flat bar was attached at both ends to the nodes "f" (Fig. 1), which were later replaced in static calculations (Section 6) with elastic supports.

The introduced axial load to the flat bar was controlled by measuring the deformation in the tie-rod using resistance wire strain gauges

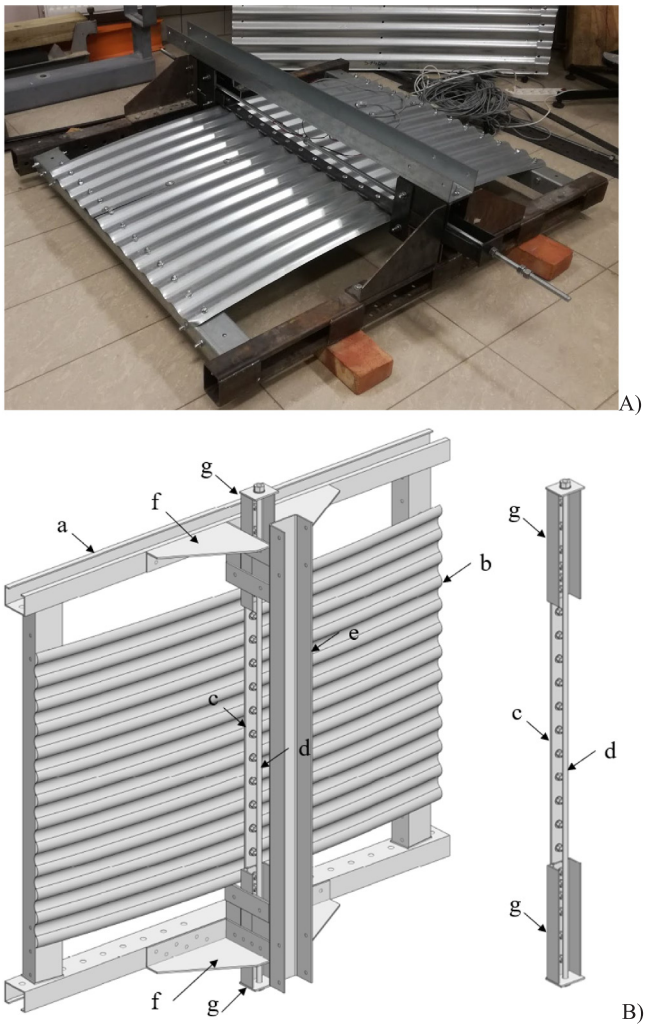

Fig. 1. Test stand of silo column connected to corrugated sheet on laboratory scale ((A) view and (B) scheme): (a) steel frame, (b) corrugated sheet, (c) column-flat bar with cross-section of 50 × 6 mm^2, (d) steel tie-rod M16, (e) C-profile stiffening steel frame, (f) outermost rigid support nodes and (g) C-profile connecting flat bar with tie-rod.

with a resistance of 120 Ω glued to the properly prepared surface of the threaded tie-rod. Based on the measured deformations, the tie-rod cross-section (diameter 16 mm) and Young's modulus of the steel (210 GPa), the force acting in the tie-rod was determined. Additionally, the outermost displacements of the flat bar nodes were measured with the use of two inductive sensors of the Peltron PS×20 type. The difference in the distance caused by tie-rod compression was measured between the stiff node "f" and the profile connecting the flat bar to the tie-rod "g" (Figs. 1 and 2). The data acquisition system was the 8-channel universal measurement amplifier Quantum. Measurement results were recorded with a frequency of at least 0.5 Hz.

2.2. Real silo

The entire experimental stand-up consisted of two full-scale steel cylindrical silos with a capacity allowing the storage of 35 tons of wheat in each of the silos. One of the silos was used to perform the experiments (Fig. 3A), while the other silos stored wheat. The silos were designed and used to measure the pressure of bulk material against the silo wall during gravity filling and emptying [28]. The height of the cylindrical part of the silos was 7.6 m, and the diameter was 2.68 m. The radius of the cylindrical wall (R = 1340 mm) was about 4.7 times

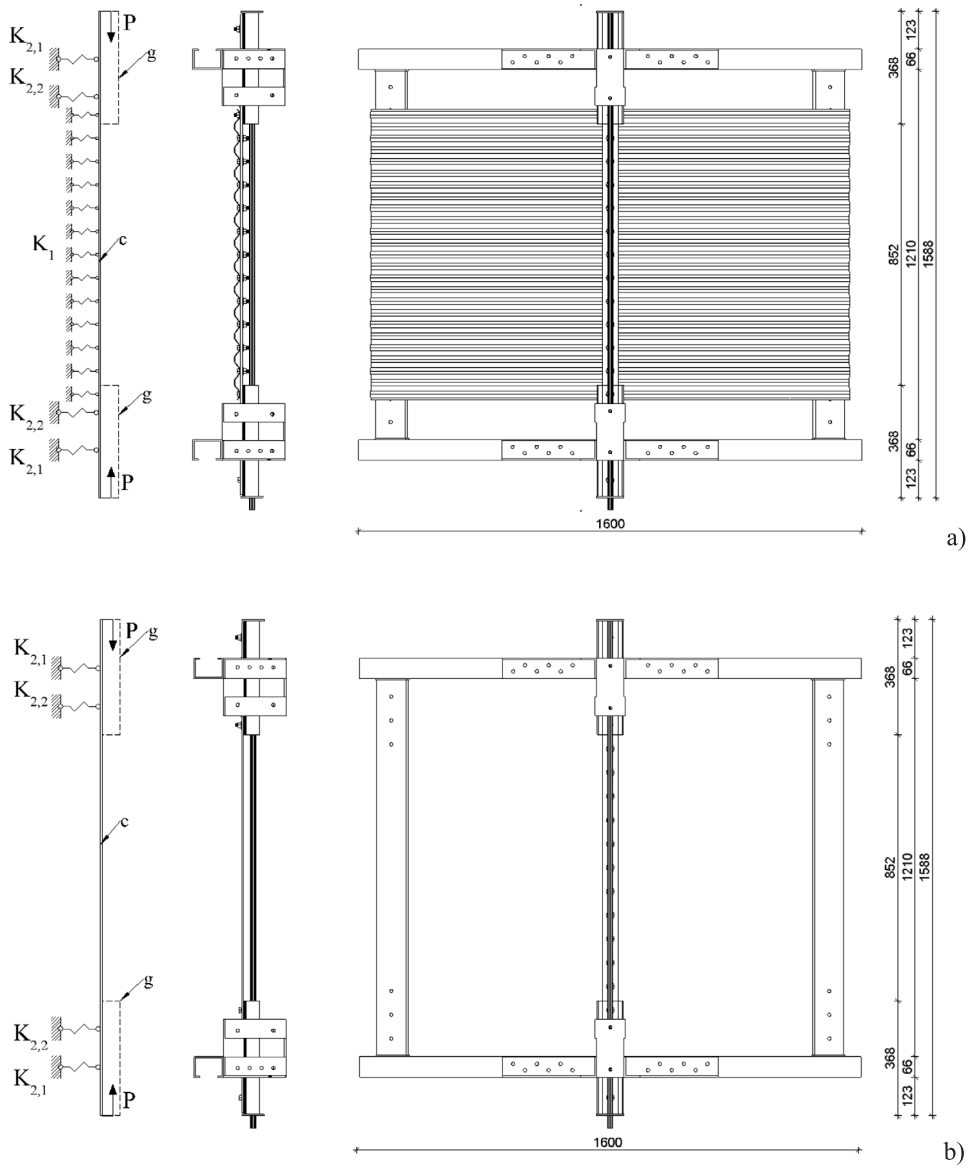

Fig. 2. Static scheme of silo fragment test stand-up at laboratory scale: (a) with corrugated sheet and (b) without corrugated sheet ((c) — flat bar with cross-section of 50 × 6 mm^2, (g) C-profile connecting flat bar with tie-rod M16, P — compressive force in flat bar introduced by tie-rod, K_1 — elastic foundation in form of corrugated sheet, $K_{2.1}$ and $K_{2.2}$ — elastic supports).

smaller than in the laboratory. The silos were made of corrugated sheets 0.75 mm thick, stiffened with six vertical columns spaced 1.4 m along the perimeter. The vertical columns were made of thin-walled C-profiles with a wall thickness of 1.5 mm and 4 mm. The silo had a conical roof with a slope of 25°. Two horizontal bulk material conveyors (upper and lower redler with a capacity of 150 t/h) and a vertical bucket elevator were used to fill the silos. Emptying the silos was done by gravity. Due to the dimensions of the structure and the possibility of introducing the failure load, the experiments were performed for a single column that was modified as compared to the original one (C-profile). A flat bar of 50 × 6 mm^2 (the same as in laboratory tests) was adopted at a height of 0.84 m to 3.33 m, measured from the junction of the silo mantle with the conical hopper. The flat bar was connected to the silo shell along its entire height with screw connectors with a spacing of 76 mm (equal to the corrugated sheet wavelength). Fig. 3B shows a schematic of the experimental stand-up, in which the existing thin-walled C-column at a height of 2508 mm was dismantled. A rigid node "*f*" was attached to the remaining part of the existing column "a", which rigidly connected the movable element of the test stand-up in the form of a C-profile "*e*" placed inside while allowing freedom of displacements along the load axis. The C-profile "e" connected the compressed flat bar "c" with two tie-rods M16 "*d*" using which the load was introduced to the structure. The load was again introduced by hand alternately through two tie-rods as a result of the rotation of nuts. The introduced compressive load for the analysed column was measured by measuring the deformation in tie-rods (analogous to the test stand-up at the laboratory scale). Regardless of the control of the introduced compressive force, the axial force and bending moments in the mid-span of the flat bar were also controlled. The internal forces in the flat bar were determined based on the measurement of deformations on the outermost opposite flat bar cross-sections. The deformation was determined using two resistance wire strain gauges with a resistance of 120 Ω. Based on the geometry of the cross-section of the flat bar and Young's modulus of steel (210 GPa), the stress distribution in the cross-section of the flat bar was determined, followed by the internal forces (axial force and bending moment). Two inductive displacement sensors

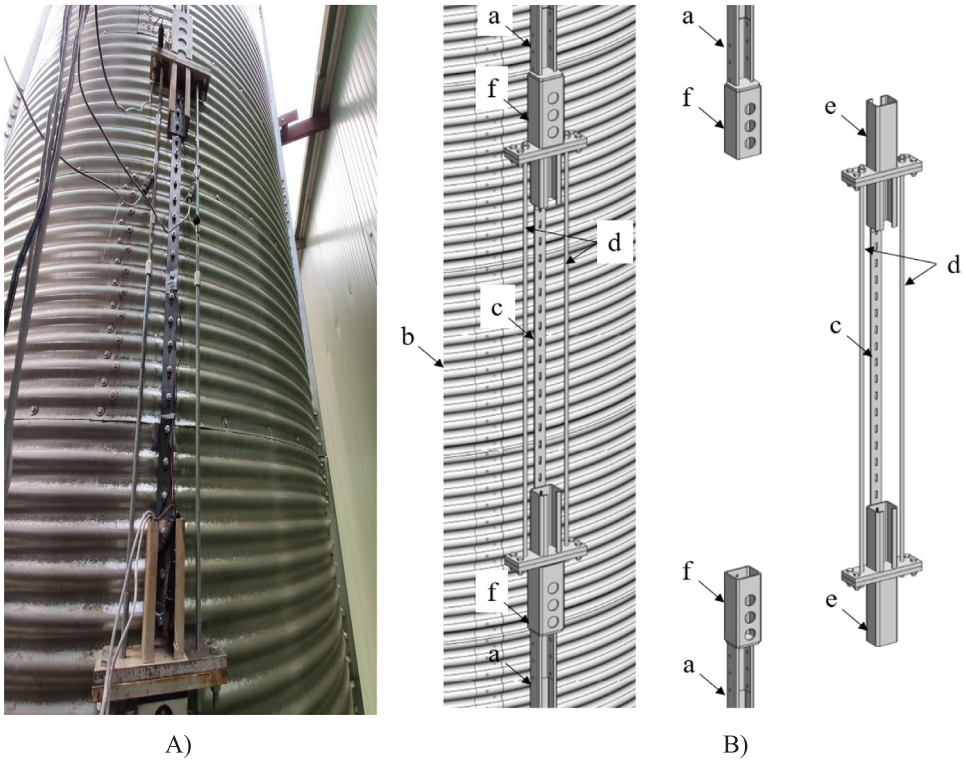

Fig. 3. Experimental silo ((A) view and (B) scheme): (a) C-profile column with thin-walled section, (b) corrugated sheet, (c) flat bar with cross-section of 50 × 6 mm^2, (d) two M16 steel tie-rods, (e) C-profile connecting flat bar with tie-rod and (f) outermost rigid support nodes.

of the Peltron PS×20 type (transformer linear displacement transducer LVDT) were used to measure the displacements. Displacement sensors were placed at fixed nodes "*f*", measuring the difference in distance between the movable element "*e*" and the fixed element "*f*".

2.3. Geodetic measurements in real silo

To determine the amplitude of initial geometrical imperfections, a scan of the silo stand was performed using a 3D laser scanner "Leica ScanStation C10". Fig. 4a presents the view of the grid of measurement points for the entire test stand, based on the ground-based laser scan of the structure (the silo was empty). Due to the difficult measuring access to the experimental column (column S_1 in Fig. 4b), the geometric imperfections were analysed in detail on the adjacent column S_2 and a fragment of the silo shell 1.0 m wide between vertical sections "A" and "B" close to the column S_1 (Fig. 4b). The obtained geometry was then compared with the surface of an ideal cylinder inscribed in the silo base and presented in the form of a deviation map of the actual geometry of the analysed fragment of the silo shell. Additionally, preliminary geometric imperfections of the adjacent column (column S_2 in Fig. 4b) were analysed and compared with the surface of an ideal column in the form of a C-profile (Fig. 4c). Fig. 4d shows the vertical sections "A" and "B" through the silo shell along with the actual geometry deviations from the ideal cylinder geometry and the deviations of the adjacent column S_2 in the radial (outside the silo) direction. In the vicinity of the analysed column (cross-section "B" in Fig. 4b), a horizontal deviation from the vertical of the actual structure of the silo shell equal to approx. w=10–15 mm was observed. The maximum deviation of the silo shell from the vertical was about w = 30 mm and occurred in its upper part. The maximum amplitude of the imperfection of the corrugated sheet in the close vicinity of the measuring column was approximately 15 mm. The measured amplitude, w = 15 mm, was used in the FE calculations for the empty and pre-filled silo (Section 6).

3. Experimental results

3.1. Experiments with column with corrugated sheet on laboratory scale

The results of the experimental tests on a laboratory scale are presented in Fig. 5. Fig. 5A shows the dependence of the compressive horizontal force N in the tie-rod on the introduced horizontal displacement u for a column with a corrugated sheet ('*a*' curve) and for a column without a corrugated sheet '*b*' curve) for one exemplary test (during loading and unloading).

The distortions in force–displacement diagrams happened because the flat bar was compressed by hand tightening the tie-rod. The maximum force for a column with a corrugated sheet was N = 16.5 kN (curve '*a*'). In the case of a column without a corrugated sheet, the maximum force N was lower by about 50%, i.e. 8.4 kN (curve '*b*'). The deformation of the analysed system under the influence of the load is shown in Fig. 5B for a column with a corrugated sheet (u = 15.5 mm) and a column without a corrugated sheet (u = 22.7 mm). The experiments were performed on 8 trials, in which similar results were obtained (a maximum difference was 7%–10%). The deformation of the column with a corrugated sheet (Fig. 5Ba) and without a corrugated sheet (Fig. 5Bb) corresponded to a half-wave with a plastic hinge in the mid-span of the compressed flat bar "*c*" and in connections of the flat bar with the C-profile "*g*" (Fig. 1). Without the corrugated sheet, 1.5-times greater deformation was achieved for a twice lower failure force.

The standard buckling resistance of a single column with a corrugated sheet was determined with the formula for the stability of the equivalent orthotropic shell (Appendix B) (p.5.3.4.3.3 of Eurocode [12]). The standard buckling resistance (without considering plasticity) was equal to N = 47.8 kN, i.e. it was 2.5 times higher than the experimental one. When plasticity was taken into account during eccentric compression, the ultimate force was N = 8.6 kN (2 times lower than

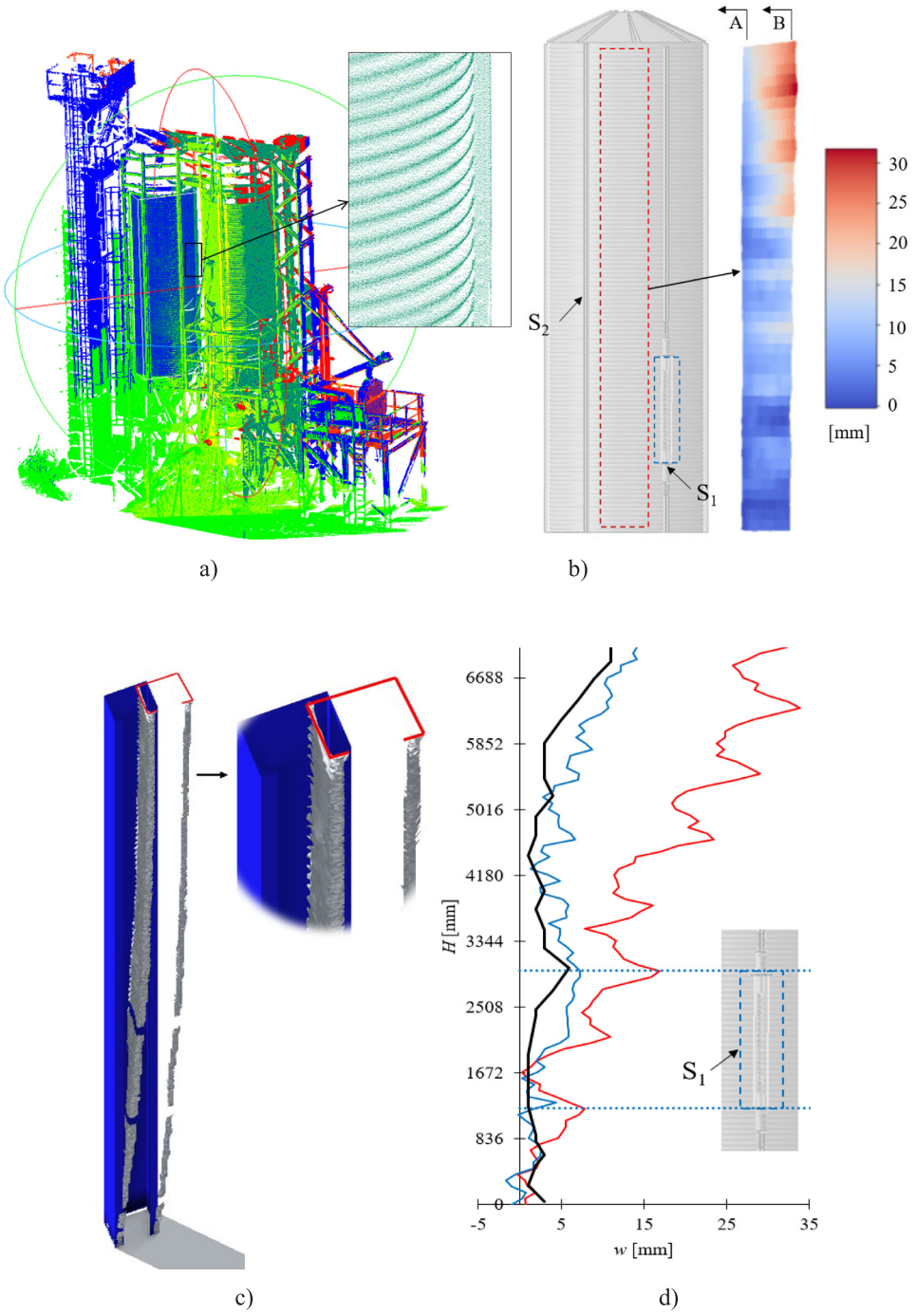

Fig. 4. Geodetic measurements of experimental real silo: (a) view of measuring points for entire test stand, (b) map of deviations (geometric imperfections) from ideal cylinder geometry for analysed fragment of silo mantle (S_1 - measuring flat bar column and S_2 - adjacent column with C-profile cross-section), (c) measured deformation of adjacent S_2 column and (d) amplitudes of initial geometric imperfections in vertical sections 'A' (blue) and 'B' (red) of fragment of silo mantle and adjacent column S_2 (black colour). (For interpretation of the references to colour in this figure legend, the reader is referred to the web version of this article.)

the experimental one). The standard buckling resistance of the single column without the corrugated sheet was $N = 7.7$ kN [29] and was 10% lower than in the experiments ($N = 8.4$ kN).

3.2. Experiments in real silo

The experiments were performed for the empty silo (2 tests) and for the pre-filled silo with wheat (2 tests), where similar results were obtained (difference up to 10%). The stability test results in the real silo are presented in Fig. 6. Fig. 6A shows the relationship between the vertical compressive force N in the tie-rod ('a' curve) and in the flat bar ('b' curve) and the displacement u (shortening) of the tie-rod for an empty silo ('E') and a silo pre-filled with wheat ('F'). The distortions in force–displacement diagrams again happened because the flat bar was compressed by hand tightening the tie-rods. Noticeable breaks in on the initial linear part of the test graphs for the tie-rod and flat bar were caused by the presence of gaps in screw connections (unavoidable in experiments). For an empty silo, the maximum measured compressive force was $N = 49$ kN (tie-rod) and $N = 39$ kN (flat bar). The difference

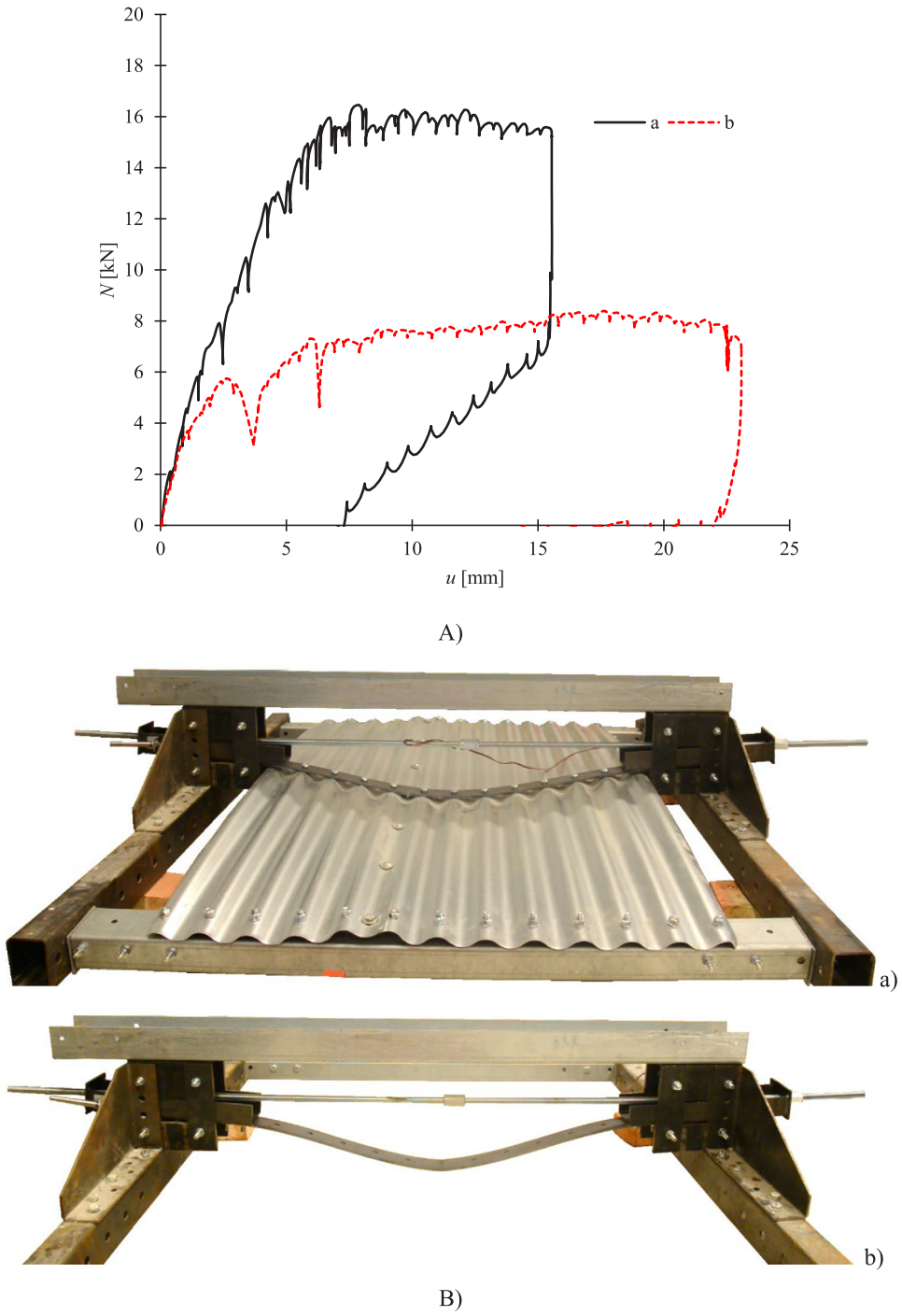

Fig. 5. Experimental tests for column at laboratory scale: (A) dependence of compressive horizontal force N in tie-rod on horizontal displacement u ('a' - column with corrugated sheet and 'b' - column without corrugated sheet) and (B) deformation of column in post-critical state ((a) with corrugated sheet for $u = 15.5$ mm and (b) without corrugated sheet for $u = 22.7$ mm).

between the compressive force measured in the tie-rod and the flat bar was because the part of the load was transferred to adjacent columns through the corrugated sheet. The presence of wheat in the silo increased the maximum compressive force up to $N = 59$ kN in the tie-rod (increase by about 20%) and up to $N = 57$ kN in the flat bar (growth by about 45%). The deformation of the analysed experimental system for the empty silo is shown in Fig. 6Ba. The flat bar with the support node in the lower and upper zones was deformed, moving inside the silo to a depth of about 40 mm (in the lower zone) and 10 mm (in the upper zone). At a distance of about 300 mm from the rigid nodes (upper and lower), a bulge appeared outside the silo with an amplitude of about 10 mm in the lower zone and 5 mm in the upper zone of the flat bar. The length of the vertical buckling half-wave was about 380 mm, which corresponded to 5 distances of screw connectors. The deformation of the silo with wheat (Fig. 6Bb) was similar to that of the empty silo but with about 4-times lower amplitude of horizontal displacements caused by the stiffness of the wheat. In addition, for this silo, there were local dents on the corrugated sheet at the place where the silo mantle connected the flat bar. The length of the horizontal buckling wave in the circumferential direction was about 700 mm.

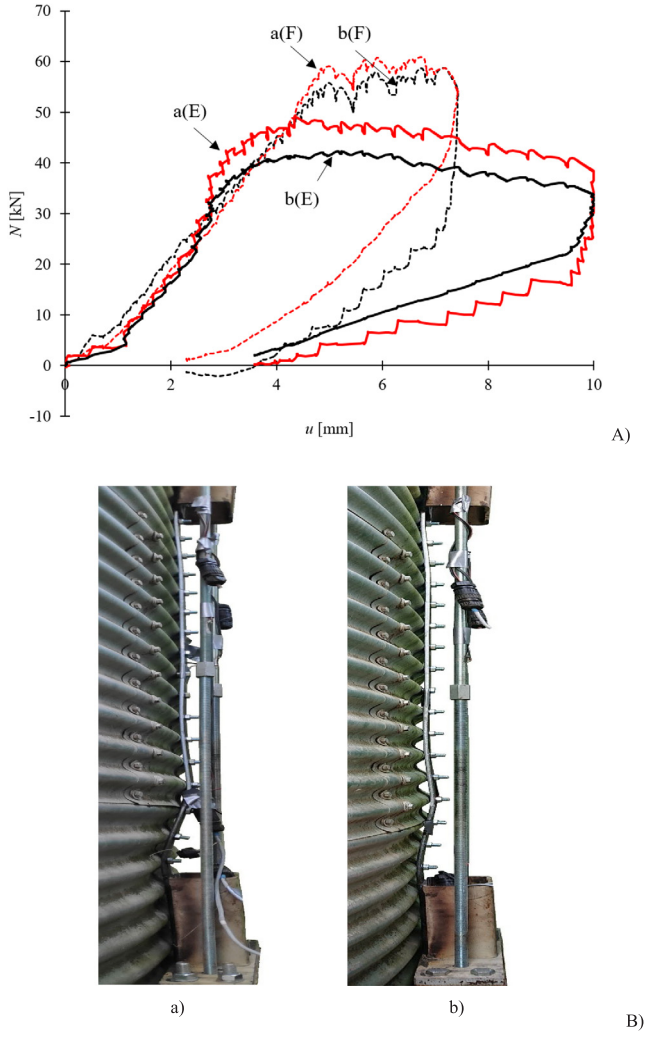

Fig. 6. Experimental tests in real silo: (A) dependence of vertical compressive force N on vertical displacement u ('a' — force in tie-rod, 'b' — force in flat bar, 'E' — empty silo and 'F' — silo pre-filled with wheat) and (B) deformation of column and corrugated sheet ((a) empty silo and (b) silo pre-filled with wheat).

The buckling resistance of a column in an empty silo was determined with code formulae for the stability of a single column based on an elastic foundation in the form of a corrugated sheet (Appendix A) (p.5.3.4.3.4 of the code [13]). The code buckling resistance was only N = 20.9 kN and was almost two times lower than the experimental one in the flat bar (39 kN). The main reason for such a clear difference comes from the incompatibility of the buckling form assumed by Eurocode [12,13] in the circumferential direction with the experimental buckling form (which was significantly smaller than this in the code for the assumed geometry of silo) (see Section 5.2).

There are no code formulae [30,31] for the buckling resistance of a column in a silo pre-filled with bulk solid.

4. Input data in FE analyses

Numerical FE analyses were carried out with the Abaqus program [32]. In numerical calculations, geometrically and material nonlinear (GMNA) analyses were performed, taking into account preliminary geometric imperfections. The following material parameters were adopted for structural steel: modulus of elasticity E = 210 GPa, Poisson's ratio υ = 0.3, and yield point f_y = 355 MPa. In the FE simulations, the elastic-perfectly plastic model of the material was adopted. To determine the dependence of loads on displacements in the structure, the implicit dynamic analysis (IDA) [33] was used, where the increase in displacements was controlled at a speed of 0.4 mm/s. The use of dynamic numerical analysis allows for a better convergence of the solution compared to static methods [17,33].

4.1. Input data for column with corrugated sheet on laboratory scale

Numerical FE simulations were carried out using two models with varying degrees of detail. In the first model (the so-called simplified model), bar elements were adopted (Fig. 7a). Two end C-profiles "g" were taken into account, rigidly connected to the flat bar "c" (Figs. 1 and 2) on the eccentricity of the connection as in the experiment. The division of bar elements into 32 finite elements was applied. The corrugated sheet was considered an elastic foundation with K_1 stiffness (Fig. 2). The stiffness of the elastic foundation was determined on the basis of the code procedure [13] (Eq. (2) in Appendix A) and the procedure proposed in [25] (Appendix C). The stiffness K_1 was determined for a sheet with a radius of R = 6240 mm, thickness t = 1.5 mm, wave length l = 76 mm, and wave height h = 18 mm. The stiffness K_1 was equal to 1.5831 N/mm^2 according to [13] and 1.6012 N/mm^2 according to [25].

The second numerical model (the so-called detailed model) (Fig. 7b) consisted of shell elements (corrugated sheet, flat bar and steel frame C-profiles) and solid elements (steel nodal plates and outermost C-profiles of the flat bar). The FE model used 4-node shell elements with reduced integration "S4R" and tetrahedral solid finite elements "C3D10" (based on previous calculations [33]). The numerical model contained a total of 155,809 finite elements. The entire steel frame rested freely at the outermost points of the steel frame. In the numerical model, the shape of the initial geometric imperfection was adopted on the basis of the observed deformations in experiments (Fig. 8a), which were obtained as a result of the analysis of photographs during the experiments. The variable amplitude of geometric imperfections ranging from 1–20 mm was assumed. Additionally, FE calculations were performed with initial geometric imperfections based on LBA (Fig. 8b).

4.2. Input data for real silo

Numerical models with two levels of detail were again adopted. The first bar model (the so-called simplified model) (Fig. 9a) reflected a single silo column with a cross-section partially changed in height to a flat bar. The corrugated sheet was defined by means of horizontal elastic supports, the stiffness of which was determined similarly to the 2D laboratory model, i.e. based on code procedures [9]. The stiffness of the linear elastic support K_1 (Fig. 2) was determined for a corrugated sheet with a radius R = 1338 mm, thickness t = 1.5 mm, wave length l = 76 mm, and wave height h = 18 mm. The stiffness K_1 was similar, i.e. K_1 = 0.57725 N/mm^2 following the standard procedure [13] and K_1 = 0.5653 N/mm^2 according to the formula in [25]. In total, 562 finite elements were used in the simplified model.

The detailed model of the silo, taking into account the entire structure of the silo with the flat bar column, is shown in Fig. 9b. The model used shell 4-node finite elements with reduced integration 'S4R' and solid tetrahedral finite elements 'C3D10' (based again on previous calculations [33]). A total of 300,939 finite elements were used in the model. The shape of the assumed geometrical imperfections for the real silo was re-assumed on the basis of deformations in the silo structure for the failure load (Fig. 10a) and in accordance with the first LBA mode (Fig. 10b). The initial amplitude of geometric imperfections was assumed in the range of 1–15 mm.

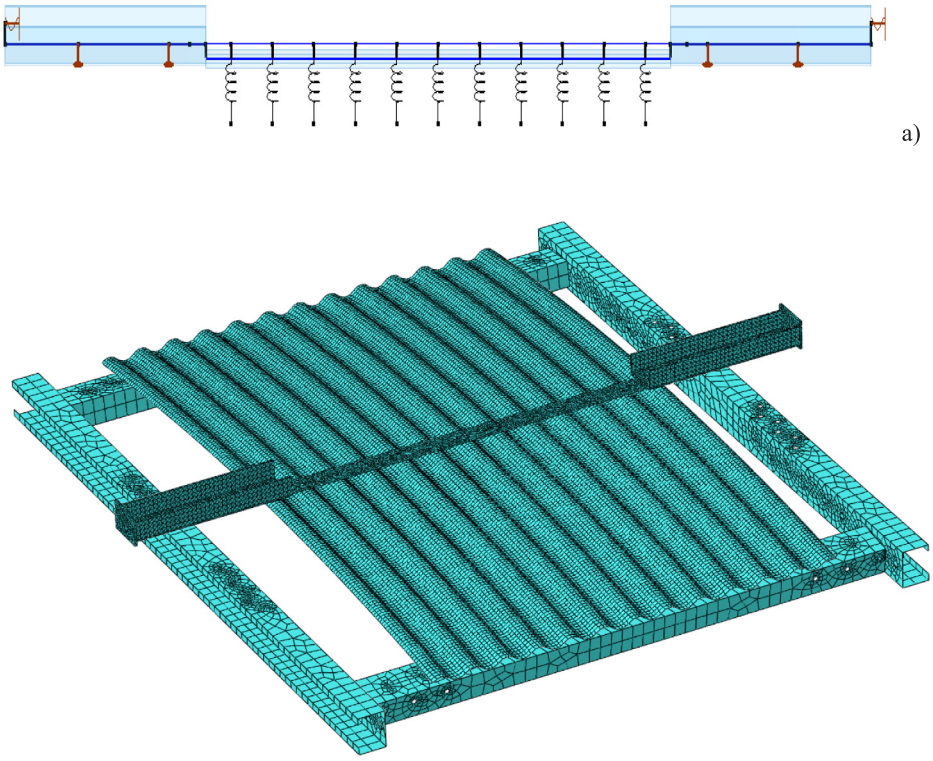

Fig. 7. Numerical FE model of silo fragment at laboratory scale: (a) simplified 2D bar model and (b) detailed 3D shell model.

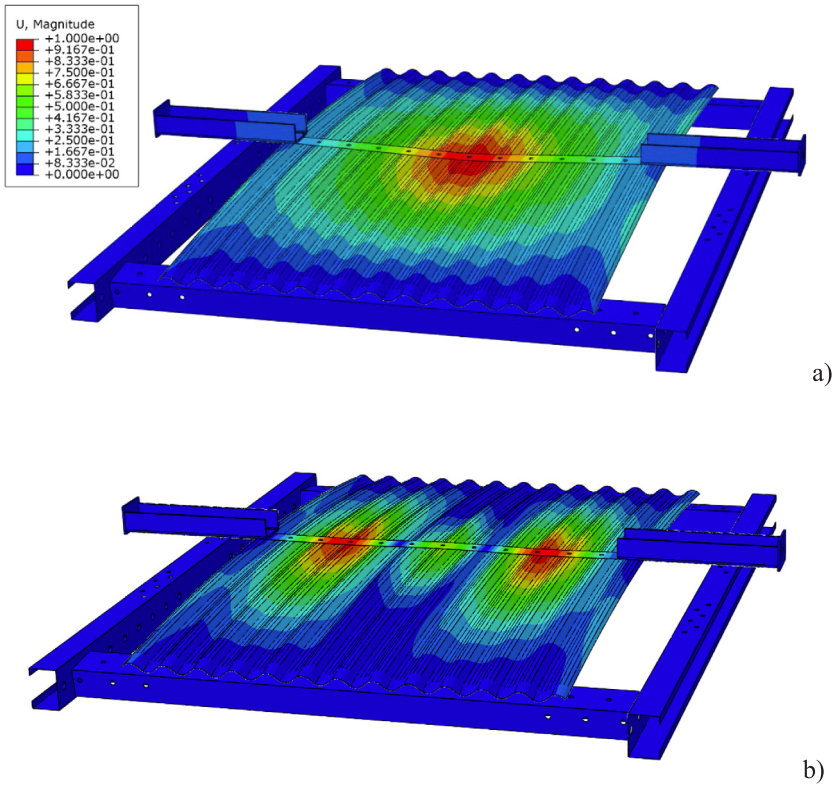

Fig. 8. Initial geometrical imperfection assumed in numerical FE simulations of experimental silo fragment at laboratory scale (detailed model) based on: (a) experimental deformation and (b) first LBA mode.

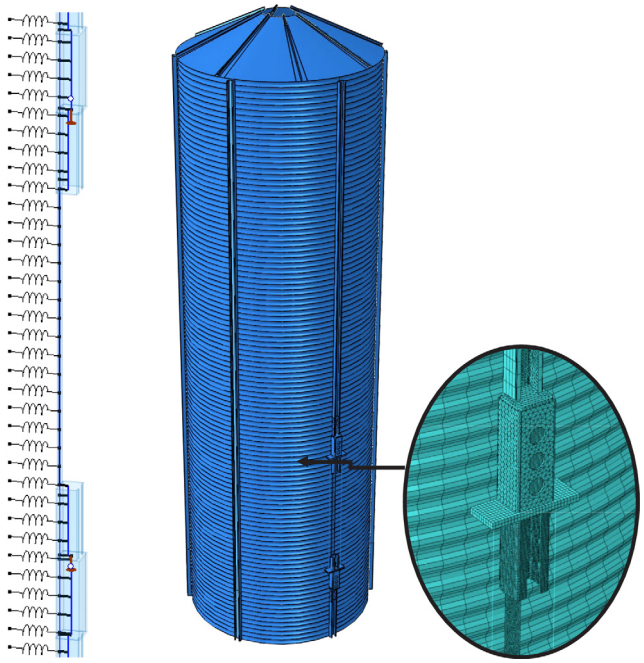

Fig. 9. Numerical FE model of real silo: (a) simplified 2D bar model and (b) detailed 3D shell model.

5. FE analysis results

5.1. FE results for column with corrugated sheet on laboratory scale

Results of FE analyses for the column without and with a corrugated sheet at the laboratory scale are presented in Figs. 11–13 (using the shell and bar model in Fig. 7).

Fig. 11 shows the dependence of the vertical compressive force N on the vertical displacement u for a detailed numerical model (Fig. 7b) with initial geometric imperfection in the form of deformation of the experimental system after failure (Fig. 8a) with initial amplitudes equal to w = 0–10 mm as compared to experimental results. The following ultimate buckling forces were calculated for the different amplitudes: N = 18.9 kN (w = 0 mm), N = 17.1 kN (w = 2.5 mm) and N = 17.0 kN (w = 10 mm). The best agreement of the numerical solution with the experimental tests (N = 16.5 kN) was, thus, obtained for w = 2.5–10 mm (5% difference). The imperfection amplitude at the level of e.g. $w \geq 2.5$ mm was consistent with the actual state. The analysed corrugated sheet segment, consisting of two overlapped sheets and a non-rigid flat bar, which had initial imperfections resulting from the processing of elements, had an impact on the formation of imperfections with an amplitude of $w \geq 2$ mm. In the case of applying the imperfection according to the first LBA mode (Fig. 8b) for the initial imperfection amplitude w = 10 mm, the ultimate compressive force N = 15.9 kN was obtained, i.e. about 7% less than in the case of imperfection being related to the deformation of the real system. For a column without a corrugated steel sheet, the compressive ultimate force from FEM was solely N = 4.0–5.0 kN (for w = 2.5–10 mm) - equal to 50%–60% of the experimental force (N = 8.4 kN). With the rigid support, the higher ultimate force N was computed as N = 6.0–8.0 kN (closer to the experimental force). The shape of deformations based on FE analyses (Fig. 12) corresponded to the experimental deformations (Fig. 5B). The calculated deformation of the column with a corrugated sheet (Fig. 12a) and without a corrugated sheet (Fig. 12b) corresponded to a half-wave with a plastic hinge at the mid-span of the flat bar "c" between points connecting the flat bar to the C-profile "g" (Fig. 1).

The FE results for the simplified 2D model (Fig. 7a) in comparison with the experimental results are presented in Fig. 13. The ultimate compressive force in the column for the initial amplitude of geometric imperfection equal to w = 0 mm was N = 42 kN, i.e. it was 2.5 times greater in relation to the experimental results (N = 16.5 kN) and to the result of the '3D' detailed model (N = 17 kN). However, it was only about 10% lower than the ultimate force on the basis of Eurocode [12] (curve 'c' in Fig. 13). The FE results similar to the experiments were obtained for the initial imperfection amplitude w = 20 mm (Fig. 13).

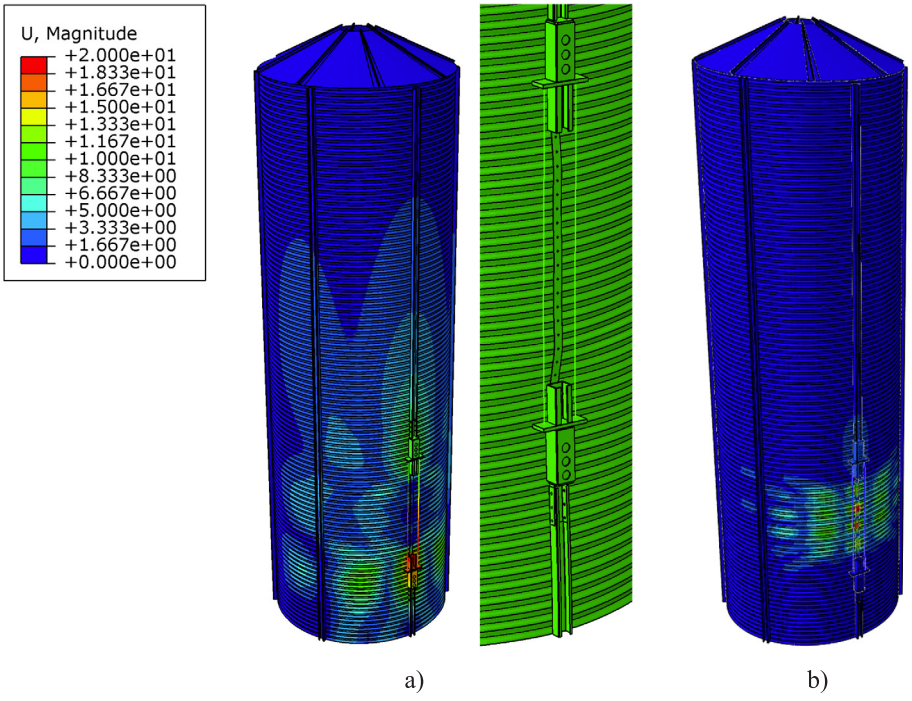

Fig. 10. Initial geometric imperfection assumed in numerical analyses of real silo (detailed model) based on: (a) experimental deformation and (b) first LBA mode.

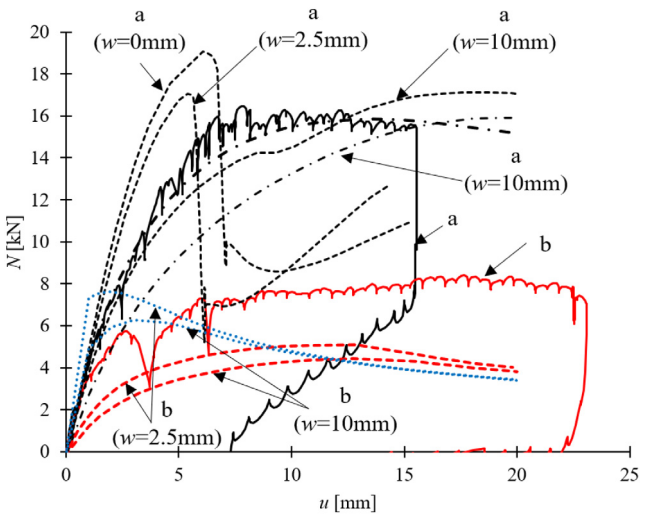

Fig. 11. FE results of detailed 3D model of silo fragment on a laboratory scale: dependence of compressive force N in tie-rod on its horizontal displacement u ((a) column with corrugated sheet, (b) column without corrugated sheet, 'continuous line' — experimental results, 'dashed line' — FE results for geometric imperfections according to Fig. 8a, dash-dot line' — FE results for geometric imperfections according to Fig. 8b 'dotted line' — FE results for geometric imperfections according to Fig. 8a for rigid support).

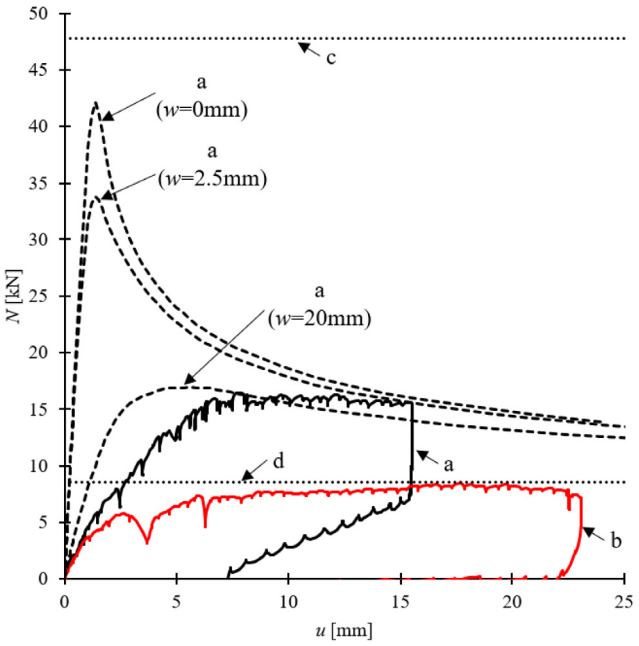

Fig. 13. FE results of simplified 2D model of silo fragment at laboratory scale: dependence of horizontal compressive force N in tie-rod on horizontal displacement u ((a) column with corrugated sheet and (b) column without corrugated sheet, 'continuous line' — experimental results, 'dashed line' — FE results, 'c' — standard buckling resistance of column with corrugated sheet [13] and 'd' — plastic bending resistance of column).

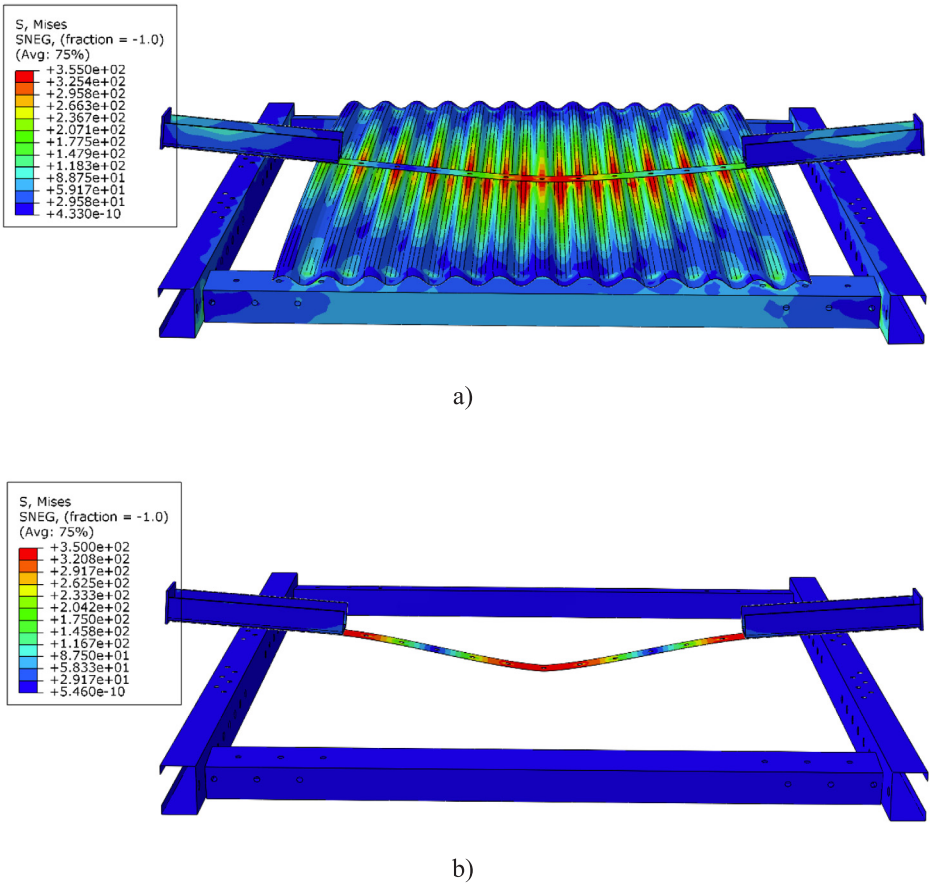

Fig. 12. FE results of silo fragment at laboratory scale: deformation with von Mises stress map [MPa] ((a) column with corrugated sheet and (b) column without corrugated sheet).

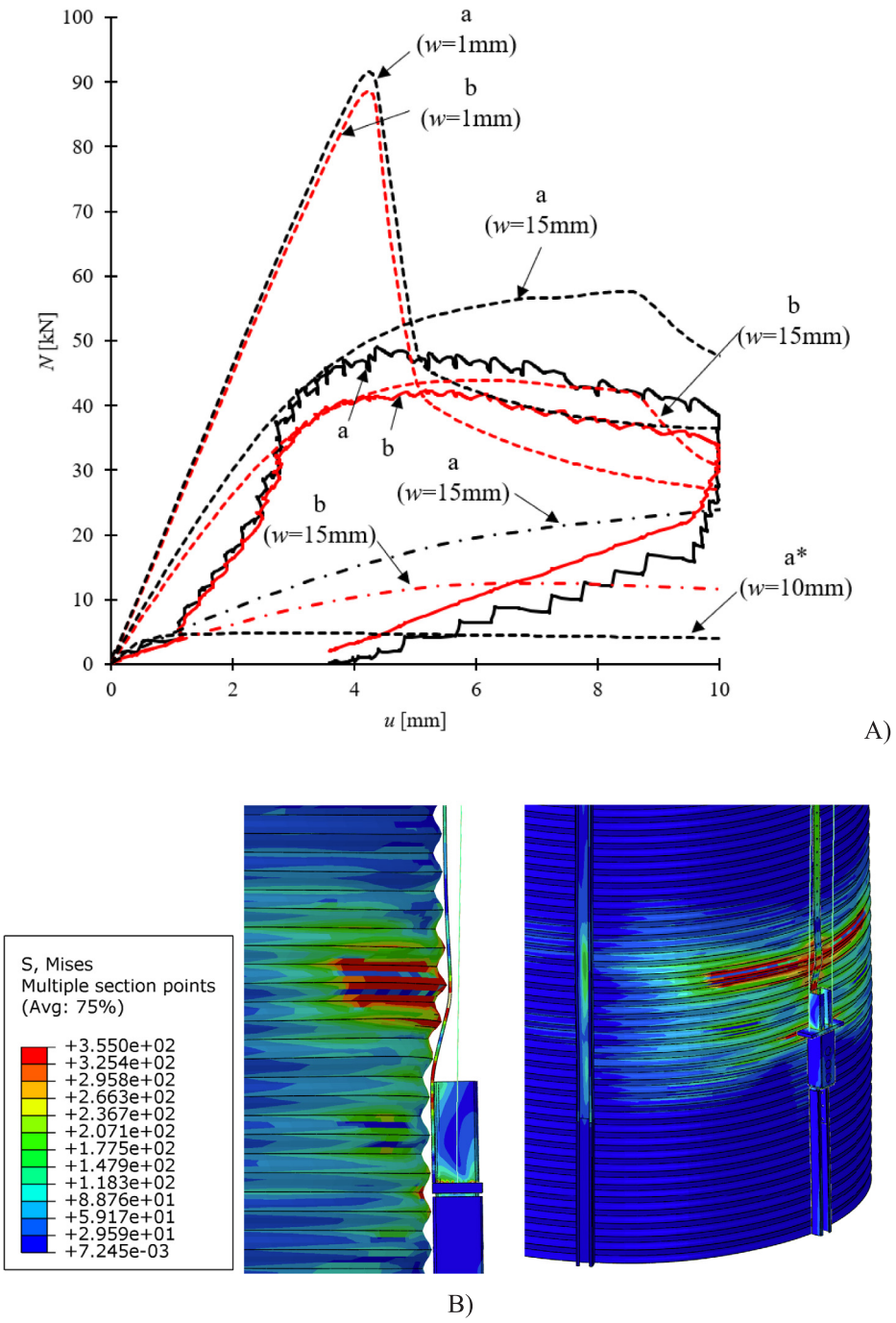

Fig. 14. FE results for 3D shell model of real empty silo: (A) dependence of vertical compressive force N in tie-rod on vertical displacement u ((a) tie-rod force, (b) flat bar force, 'continuous line' - experimental results, 'dashed line '- FE results for experimental geometric imperfection according to Fig. 10a and' dash-dot line '- FE results for geometric imperfection according to LBA (Fig. 10b), * - FE result without corrugated sheet) and (B) silo deformation with map of von Mises stresses [MPa].

5.2. FE results for real empty silo

The results of numerical analyses for a real empty silo are shown in Figs. 14 and 15 using the detailed shell model (Fig. 14) and the simplified bar model (Fig. 15) from Fig. 9.

For the detailed shell model of the empty silo with the initial amplitudes w of geometrical imperfections in the form of deformation of the experimental system at the failure (Fig. 10a), the following amplitudes were assumed $w = 1$ mm, $w = 10$ mm, and $w = 15$ mm. For the initial imperfection amplitude $w = 15$ mm (consistent with geodetic measurements, Fig. 4), the ultimate vertical forces were $N = 58$ kN in the tie-rod (dashed curve 'a') and $N = 44$ kN in the flat bar (dashed curve 'b') (Fig. 14A). Compared to the experimental tests ($N = 49$ kN and $N = 39$ kN), the higher numerical ultimate forces were obtained by approx. 20% in the tie-rod (continuous '*a*' curve) and approx. 10% in the flat bar (continuous '*b*' curve). The deformation shape based on numerical analyses of the empty silo (Fig. 14B) corresponded to the deformation in the experiments (Fig. 6) - a vertical buckling half-wave in the lower region of the flat bar (inward buckling of the flat bar at the lower node "*f*"' of Fig. 3). The length of the buckling half-wave in the circumferential direction (about 600 mm) was similar as in the experiment (about 700 mm) (Fig. 14B). For initial geometric imperfection by the first buckling mode from LBA (Fig. 10b), much lower ultimate vertical forces N (differences of 100%) were obtained

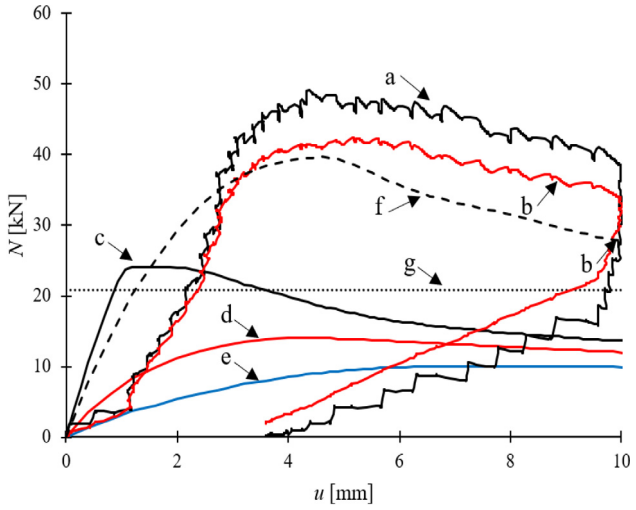

Fig. 15. FE results for simplified 2D silo model: (a) experimental force N in tie-rod, (b) experimental force N in flat bar, (c) calculated force for initial geometric imperfection amplitude $w = 0$ mm, (d) calculated force for $w = 5$ mm, (e) calculated force for $w = 10$ mm, (f) calculated force for $w = 5$ mm (modified stiffness of elastic foundation) and (g) standard buckling resistance [13] (u – vertical displacement).

for the amplitude $w = 15$ mm than for the experimental imperfection type (Fig. 14).

For the simplified numerical model (Fig. 9a), the buckling resistance was much lower compared to the experimental one and the detailed numerical model (Fig. 15). For the imperfection amplitude equal to $w = 0$ mm, the maximum force N was 24 kN (curve 'c'), i.e. 2 times lower than the experimental value. Subsequently, for the amplitudes of geometric imperfections equal to $w = 5$ and $w = 10$ mm, the maximum forces were reduced to $N = 14$ kN and $N = 10$ kN (curves 'd' and 'e'). The difference in the results of the simplified model in relation to the experimental results was caused by assuming too low stiffness of the elastic foundation according to Eurocode. Other numerical calculations based on the LBA indicated that in the tested silo there was a global buckling mode other than assumed in the standard, which was characterized by a buckling half-wave shorter than the column spacing and consistently higher stiffness of the subsoil. The curve 'f' corresponded to the simplified model for the assumed stiffness of the elastic foundation in accordance with the buckling form of the analysed silo. For the stiffness of the elastic foundation K, calculated on the basis of Eurocode, taking into account the buckling half-wave length in the circumferential direction based on LBA, the ultimate vertical force was approximately $N = 38$ kN (approximately 20% less than in the experimental tests, $N = 49$ kN). For the flat bar, not connected to the corrugated sheet, the maximum compressive force in the tie-rod was only $N = 4$ kN (curve 'a*' in Fig. 14), i.e. 10% of the buckling resistance of the column with the corrugated sheet.

Fig. 16 compares the buckling deformation form of the silo in the circumferential direction according to Eurocode [13] (corresponding to the curve 'g' in Fig. 15) and in numerical calculations using a simplified silo model (corresponding to the curve 'f' in Fig. 15). The silo schemes for calculating the stiffness of the elastic foundation K are also shown. In the numerical silo model, the 3D buckling deformation of the real silo with LBA of Fig. 10a was taken into account (Fig. 16a). The supports were assumed at the places where the buckling displacements of the 3D silo were zero for preserving the same buckling form (Figs. 16a and 16c). It may be seen that the length of the buckling half-wave in the numerical model (Fig. 16c) is significantly lower (by factor 2) than in Eurocode [13] (Fig. 16b). This length difference causes the 12-times growth of the numerical foundation stiffness K as compared to Eurocode [13].

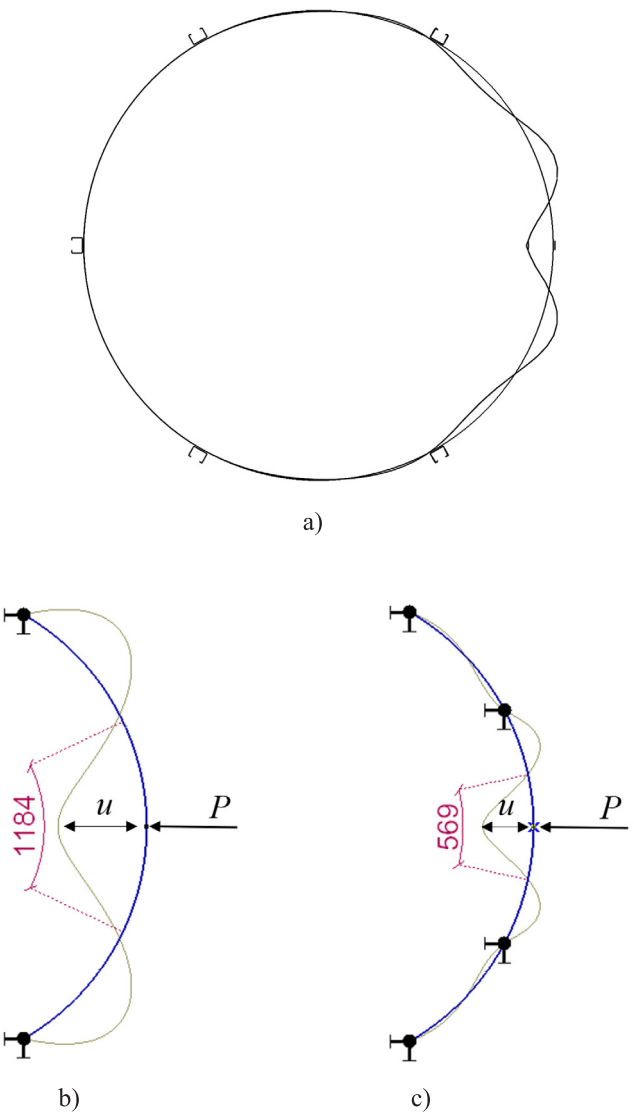

Fig. 16. Silo buckling forms in circumferential direction and simplified silo models for calculating stiffness of elastic foundation K: (a) buckling form from 3D LBA simulations (Fig. 10b), (b) Eurocode model [13] (case 'g' in Fig. 15) and (c) numerical model (case 'f' in Fig. 15) (length of buckling wave is in [mm], $K=P/u$, P - force, u - displacement).

5.3. FE results for real silo pre-filled with wheat

In numerical analyses of the real silo, the behaviour of wheat was taken into account in a simplified way. In the first case, the elastic Winkler–Pasternak foundation and in the second case, elastic solid finite elements were used. The use of a nonlinear model in a stability analysis to describe the complex behaviour of bulk solids, by taking into account the effect of density, pressure, and direction of deformation (using a hypoplastic constitutive law [34]) was described in [30,31]. The stability simulations with a non-linear hypoplastic model are more realistic but extremely time-consuming (they are foreseen in the next research step).

Winkler–Pasternak foundation

The bulk solid (wheat) was simulated as a two-parameter elastic Winkler–Pasternak foundation (Fig. 17a). For this foundation, horizontal springs with a constant K_W defined the stiffness of the Winkler foundation and inclined springs with a constant K_P defining the stiffness of the Pasternak foundation were defined. The elastic constants K_W and K_P were determined from the analysis of the axial-symmetric

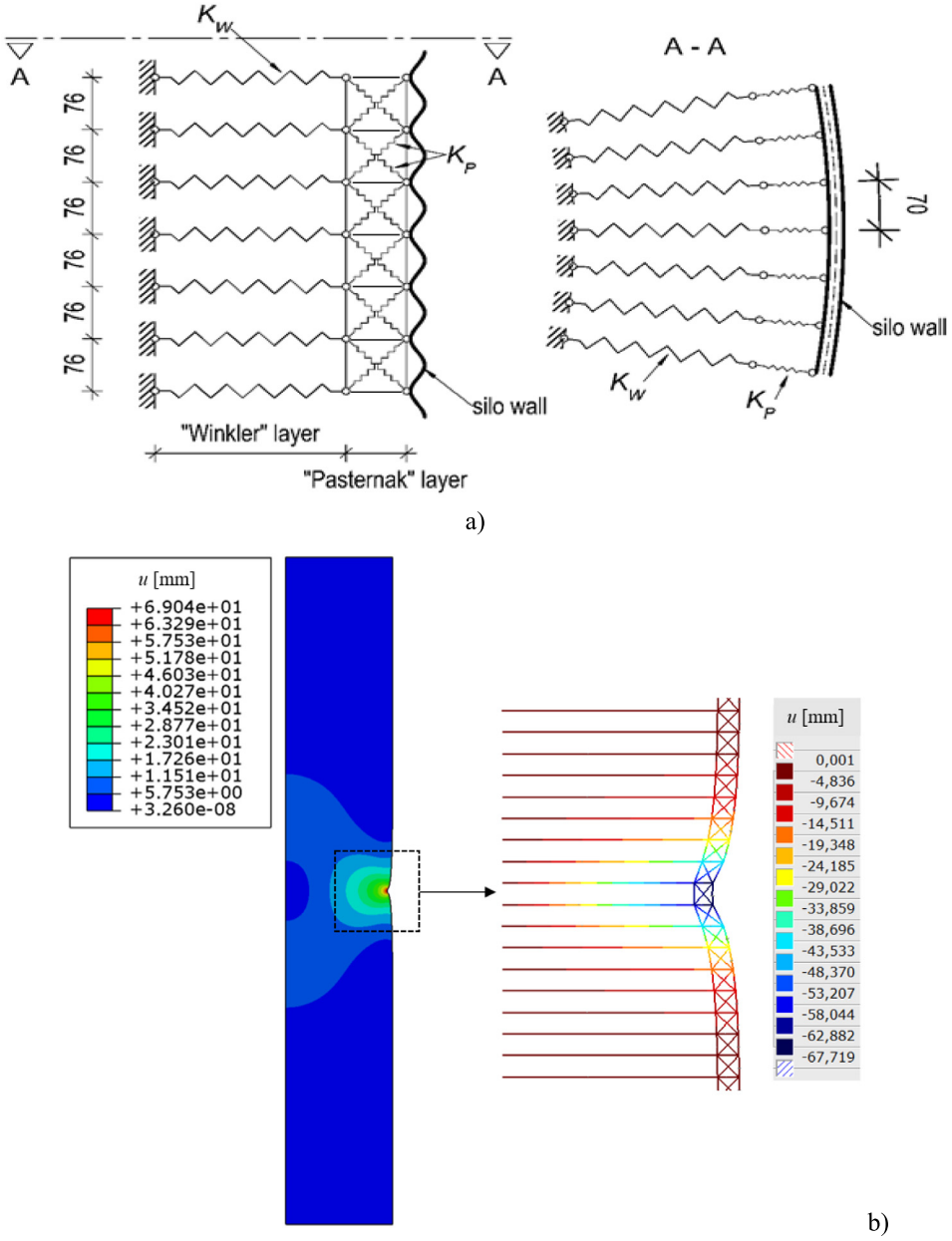

Fig. 17. Axial-symmetric Winkler–Pasternak foundation: (a) scheme and (b) test for equivalent elastic Winkler–Pasternak foundation from unit concentrated load (displacement u [mm]).

displacements of the numerical model of the bulk material inside the silo and loaded with unit values of a linear load of 1 N/mm and a local load of the same value distributed over a length of 76 mm. The effective modulus of elasticity of the bulk solid E_{sU} for the simplified model was determined according to the formula [11]:

$$E_{sU} = \chi \cdot p_{vft}, \tag{1}$$

where p_{vft} – the vertical component of bulk material pressure and χ - the calibration coefficient expressed by the formula $\chi = 7\gamma^{3/2}$, where γ is the volumetric weight of the stored [kN/m^3]. The effective modulus of elasticity of wheat was $E_{sU} = 2.76$ MPa. Its value was determined for the vertical component of the bulk material pressure $p_{vft} = 16.62$ kPa [11] in the mid-span of the compressed flat bar. The Winkler's foundation stiffness was equal to $K_W = 15.26$ N/mm:

$$K_W = k_W \cdot l_1 \cdot h_1 \tag{2}$$

with

$$k_w = p/u_{linear}, \tag{3}$$

where $l_1 = 70$ mm – the spacing of nodes along the silo circumference, $h_1 = 76$ mm – the spacing of nodes in the wave valleys of the corrugated sheet, $p = 1$ N/mm^2 – the unit load, $u_{linear} = 348.7$ mm – the calculated displacement in the axially-symmetric numerical model of the bulk solid for a unit load p. The stiffness of the Pasternak foundation was assumed to be $K_P = 74.77$ N/mm. This value was determined by a calibration process in such a way that the displacements in the equivalent Winkler–Pasternak foundation from the unit local load were consistent with the displacements obtained in the axial-symmetric numerical model of the bulk solid. For the assumed stiffness of the Winkler–Pasternak foundation, a comparative deformation analysis of the foundation under the influence of a unit concentrated load was carried out in comparison to the deformation obtained for the

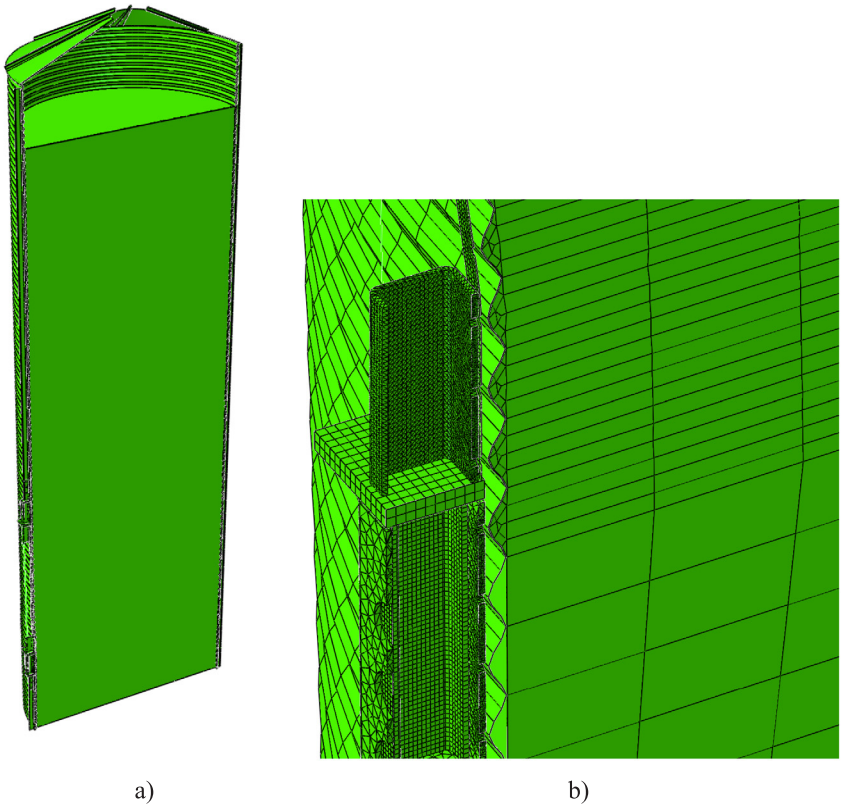

Fig. 18. Continuum FE model for bulk solid: (a) cross-section view and (b) detailing of FE mesh in region of analysed column.

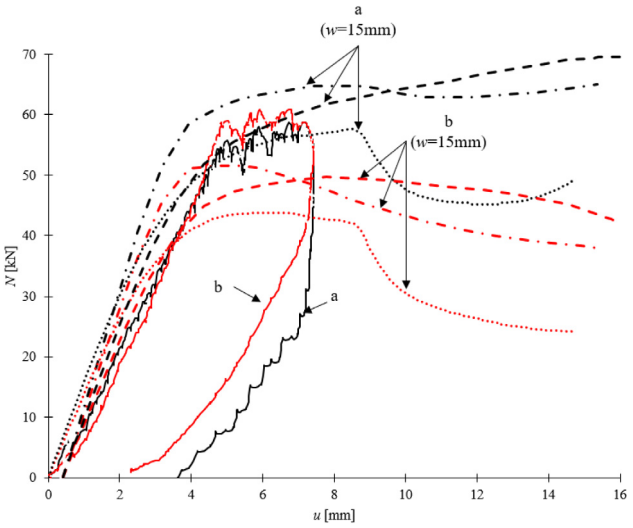

Fig. 19. FE results for detailed 3D model of real silo with wheat: dependence of vertical compressive force N on vertical displacement u ('a' — force in tie-rod, 'b' — force in flat bar, 'continuous line' — experiments, 'dotted line' — without silo fill, ' dash–dot line' — FE result with elastic Winkler–Pasternak foundation and 'dashed line' — FE result with elastic solid elements).

axial-symmetric material model under plane strain (Fig. 17b). The displacement differences were solely 2%.

Solid finite elements

An elastic continuum model for wheat consisting of 3D solid finite elements was adopted (Fig. 18a). The material stiffness for solid elements was assumed as for the Winkler–Pasternak model (with Young's modulus E_{Su} = 2.76 MPa by Eq. (1)). The solid model of wheat was adjusted to the shape of the corrugated sheet in the horizontal plane of the analysed column (Fig. 18b). In the remaining fragments, the wheat came into contact with the corrugated sheet only in its valleys.

For the analysed elastic models, both the Winkler–Pasternak model and the solid continuum, model, the contact between the elastic foundation and the surface of the corrugated sheet was used that assumed that the mutually contacting surfaces of the silo fill and walls might undergo separation despite initial connection. The occurrence of tensile stresses in wheat was excluded.

FE results

The FE analyses for the silo with wheat were carried out for a detailed numerical model with the initial amplitude of geometric imperfections w = 15 mm (Fig. 9b), based on geodetic measurements for the empty silo (Fig. 4). The dependence of the compressive force N on the vertical displacement u is shown in Fig. 19.

The compressive force in the tie-rod increased in calculations up to N = 69 kN for the solid model (the dashed curve 'a' in Fig. 19) and up to N = 65 kN for the elastic Winkler–Pasternak foundation (the dash-dot curve 'a' in Fig. 19). As compared to the empty silo (N = 58 kN), the calculated increase of the force N in the tie-rod (by about 10%–20%) was lower than in the experiments (by 20%). The calculated compressive force in the flat bar was lower and amounted to N = 50 kN (solid model) and N = 52 kN (Winkler–Pasternak foundation) (dashed and dash-dot curves 'b' in Fig. 19), which caused

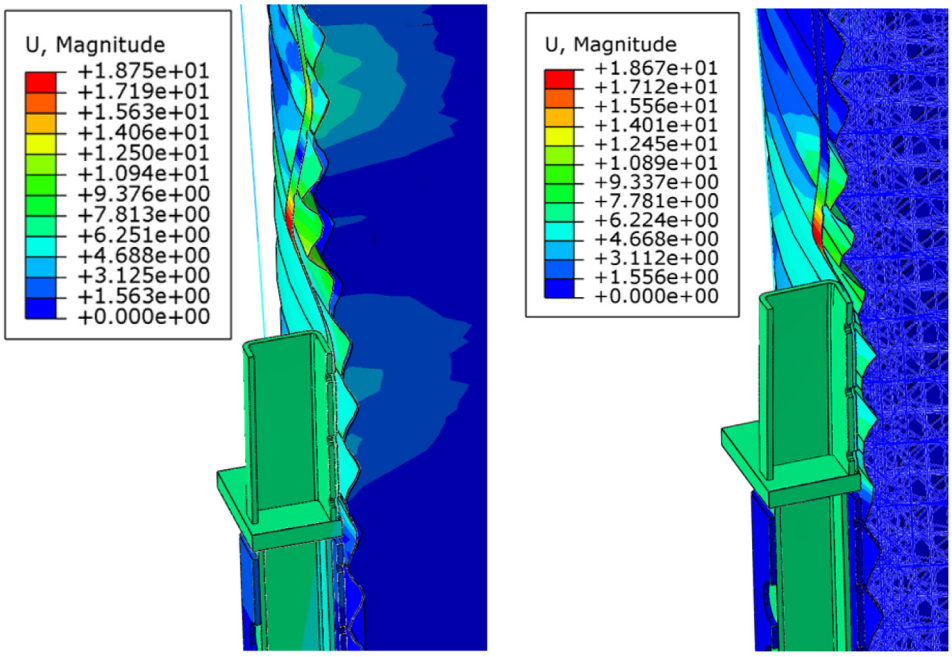

Fig. 20. FE results for real silo with wheat: deformation with global displacement map [mm] ((a) Winkler–Pasternak elastic foundation model and (b) elastic foundation in form of solid elements).

an increase as compared to the empty silo (N = 44 kN) by about 15%–20% (less than in the experiments where it was 45%). As compared with the experimental results of N (N = 49 kN and N = 39 kN), the computed mean buckling resistance was higher by about 35% in the tie-rod and by 30% in the flat bar. The numerical curves N = f(u) are slightly different for two elastic models of wheat with w = 15 mm (Fig. 19) due to a different spacing of springs and size of solid finite elements.

The deformations obtained on the basis of numerical analyses are shown in Fig. 20a (solid continuum model of wheat) and Fig. 20b (Winkler–Pasternak foundation). The obtained length of the buckling half-wave was approximately 340 mm (Fig. 20a) for the model with solid finite elements and approximately 300 mm (Fig. 20b) for the Winkler–Pasternak bedding model (on average respectively 5% and 27.5% less than in experiments, Fig. 6b). Better accordance of the deformation with the experiment (Fig. 6a) was obtained, thus, for solid finite elements.

For the empty silo and the silo pre-filled with the bulk solid, the calculated length of the buckling half-wave in the circumferential direction was approximately two times smaller than assumed in the Eurocode procedure. Therefore, the buckling resistance calculated by Eurocode was underestimated.

The reasons for discrepancies between experimental and numerical results of the compressive force N are probably caused by the assumption of a too high initial amplitude of geometric imperfections w in the pre-filled silo. In those silos, bulk solid pressure usually smoothens existing geometric imperfections [5]. For the amplitude w = 7.5 mm, the calculated force N = 60 kN in the flat bar was 20% higher than for w = 15 mm (N = 52 kN), and the buckling resistance was solely 10% lower than in the experiment.

6. Conclusions

Based on the conducted experiments and non-linear stability FE calculations, the following conclusions can be offered concerning the buckling resistance of single columns with corrugated sheets in silos:

- The presence of wheat in the silo increased the buckling resistance of the column by about 45% in the experiments. The increase in the buckling resistance of the column in FE computations resulting from the adoption of a linear elastic foundation simulating wheat was less (15%–20%), caused probably by the assumption of the too high amplitude of initial geometric imperfections.
- The buckling resistance of the real silo without a bulk solid by Eurocode 3 was two times lower than the experimental one (following the standard procedure for the sparse column spacing for which the silo qualified). Thus, the Eurocode formula needs further improvements. The most similar results obtained in the FE analyses of the empty silo compared to the experiments (differing by 10%–20%) were obtained for the 3D shell model with the initial geometric imperfection shape from the experiment (with the amplitude equal to 15 mm). The bar model of the column was two times less accurate than the shell model.
- The length of the buckling half-wave in the circumferential direction obtained in the experiments in the real silo and numerical analyses of those experiments was about two times shorter than thus assumed by Eurocode 3. The higher circumferential length of the buckling half-wave caused the lower buckling resistance.
- The assumption of initial geometrical imperfections corresponding to the first LBA mode with the amplitude of 15 mm resulted in a too extensive reduction of the buckling resistance (by 100%) as compared to the imperfections consistent with the experimental structure deformation at the failure.
- The experimental buckling resistance of a single column with a corrugated sheet on a laboratory scale was two times higher than that of a column without a sheet in tests at the laboratory scale. Without the corrugated sheet, 1.5-times greater deformation of the column was achieved for a twice lower failure force.

CRediT authorship contribution statement

K. Rejowski: Software, Investigation, Formal analysis, Data curation. **P. Iwicki:** Validation, Methodology, Conceptualization. **J. Tejchman:** Supervision, Methodology, Funding acquisition, Conceptualization. **M. Wójcik:** Methodology, Investigation.

Declaration of competing interest

The authors declare that they have no known competing financial interests or personal relationships that could have appeared to influence the work reported in this paper.

Data availability

Data will be made available on request.

Acknowledgements

The financial support of the Polish National Science Centre (NCN) in the frame of Grant No. 2011/01/B/ST8/07492 "*Safety and optimization of cylindrical metal silos containing bulk solids with respect to global stability*" and the Polish National Centre for Research and Development (NCBR) in the frame of Grant POIG.01.03.01-00-099/12 "*Innovative method of dimensioning and construction of large industrial silos made from corrugated sheets*" is gratefully acknowledged.

We would like to thank Dr. J. Szulwic from the Gdansk University of Technology for making geodetic measurements.

The numerical calculations were performed using the computing resources of CI TASK at the Gdańsk University of Technology.

Appendix A

Code formulae for calculating the stability of a single column based on an elastic foundation in the form of a corrugated sheet for a large column spacing [13]: (see Box I).

$$N_{b,Rk} = 2\sqrt{EJ \times K}, \tag{A.1}$$

with

$$\phi = \frac{d_s}{r}, \tag{A.3}$$

$$f = \frac{1}{4}\left\{(4g^2+1)(2\phi+\sin 2\phi) + 4g(1-\cos 2\phi) - 2\sin 2\phi\right\}, \tag{A.4}$$

$$g = \frac{D_y \sin^2\phi - r^2 C_y\left[(1-\cos\phi)(1+3\cos\phi) - \phi\sin 2\phi\right]}{D_y(2\phi+\sin 2\phi) - r^2 C_y\left[2\phi(2+\cos 2\phi) - 3\sin 2\phi\right]}, \tag{A.5}$$

where

EJ - the flexural rigidity of the stiffener for bending out of the plane of the wall,

C_y - the shell membrane stiffness of the corrugated wall sheet for circumferential stretching,

D_y - the shell bending flexural rigidity of the corrugated wall sheet for circumferential bending,

d_s - the circumferential separation of vertical columns,

r - the silo radius.

$$K = \frac{1}{r}\left\{\frac{2C_y D_y}{f D_y + r^2 C_y\left\{f + \phi\cos^2\phi(\tan\phi+2g)^2 - 2\left[2g^2\sin 2\phi - 2g(\cos 2\phi - \cos\phi) - \sin\phi(\cos\phi - 1)\right]\right\}}\right\}, \tag{A.2}$$

Box I.

Appendix B

Code formulae for calculating the stability of the equivalent orthotropic shell for a small column spacing [12]:

$$n_{x,Rcr} = \min\left(\frac{1}{j^2\omega^2}\left(A_1 + \frac{A_2}{A_3}\right)\right) \tag{B.1}$$

with

$$\omega = \frac{\pi r}{j l_i}, \tag{B.2}$$

$$A_1 = j^4\left[\omega^4 C_{44} + 2\omega^2(C_{45}+C_{66}) + C_{55}\right] + C_{22} + 2j^2 C_{25}, \tag{B.3}$$

$$A_2 = 2\omega^2(C_{12}+C_{33})(C_{22}+j^2C_{25})(C_{12}+j^2\omega^2 C_{14}) - (\omega^2 C_{11}+C_{33})(C_{22}+j^2C_{25})^2 - \omega^2(C_{22}+\omega^2 C_{33})(C_{12}+j^2\omega^2 C_{14})^2, \tag{B.4}$$

$$A_3 = (\omega^2 C_{11}+C_{33})(C_{22}+C_{25}+\omega^2 C_{33}) - \omega^2(C_{12}+C_{33})^2, \tag{B.5}$$

$$C_{11} = C_\phi + EA_s/d_s, \tag{B.6}$$

$$C_{12} = \upsilon\sqrt{C_\phi C_\theta}, \tag{B.7}$$

$$C_{14} = \frac{e_s EA_s}{(rd_s)}, \tag{B.8}$$

$$C_{44} = \frac{\left[D_\phi + \frac{EI_s}{d_s} + \frac{EA_s e_s^2}{d_s}\right]}{r^2}, \tag{B.9}$$

$$C_{22} = C_\theta + EA_r/d_r, \tag{B.10}$$

$$C_{33} = C_{\phi\theta}, \tag{B.11}$$

$$C_{25} = \frac{e_r EA_r}{(rd_r)}, \tag{B.12}$$

$$C_{55} = \left[D_\theta + \frac{EI_r}{d_r} + \frac{EA_r e_r^2}{d_r}\right]/r^2, \tag{B.13}$$

$$C_{66} = \left[D_{\phi\theta} + 0,5\left(\frac{GI_{ts}}{d_s} + \frac{GI_{tr}}{d_r}\right)\right]/r^2, \tag{B.14}$$

where

l_i — the half wavelength of the potential buckle in the vertical direction,

j — the critical circumferential wave number of the potential buckle form,

A_s — the cross-sectional area of a stringer stiffener,

I_s — the second moment of area of a stringer stiffener about the circumferential axis (vertical bending),

d_s — the separation between stringer stiffeners,

I_{ts} — the uniform torsion constant of a stringer stiffener,

e_s — the outward eccentricity from the shell middle surface of a stringer stiffener,

A_r — the cross-sectional area of a ring stiffener,

I_r — the second moment of area of the ring stiffener about the vertical axis (circumferential bending),

d_r — the separation between ring stiffeners,
I_{tr} — the uniform torsion constant of the ring stiffener,
e_r — the outward eccentricity from the shell mid-surface of the ring stiffener,
C_ϕ — the sheeting stretching stiffness in the axial direction,
C_θ — the sheeting stretching stiffness in the circumferential direction,
$C_{\phi\theta}$ — the sheeting stretching stiffness in membrane shear,
D_ϕ — the sheeting flexural rigidity in the axial direction,
D_θ — the sheeting flexural rigidity in the circumferential direction,
$D_{\phi\theta}$ — the sheeting twisting flexural rigidity in twisting,
r — the silo radius.

Appendix C

Formulae for calculating the stiffness of the elastic foundation K proposed in [25]:

$$K = \frac{8 \cdot D_y}{Y} \tag{C.1}$$

with

$$\begin{aligned} Y = {} & r^3\left(2A_1 - 16X + 24A_1X^2 + 16B_1X\right) \\ & + r^2(-4L + 3B_1L + 16Xf - 16LX^2 - 32A_1X^2f) \\ & + r^2\left(8A_1LX - 16B_1Xf + 4B_1LX^2\right) \\ & + r\left(A_1L^2 - 2L^2\mathrm{X} + 16LX^2f - 8A_1LXf\right) \end{aligned} \tag{C.2}$$

$$X = \frac{C_2 + C_3}{C_1}, \tag{C.3}$$

$$C_1 = 4Lf + r^2\sin\left(2A_1\right) + 6A_1r^2 + 4A_1f^2 - 4Lr - 8A_1rf, \tag{C.4}$$

$$C_2 = \frac{r^2\cos\left(2A_1\right)}{2} + f\left(2r\cos\left(A_1\right) - 2r + A_1L\right), \tag{C.5}$$

$$C_3 = \frac{3r^2}{2} - 2r^2\cos\left(A_1\right) - A_1Lr + Lr\sin\left(A_1\right), \tag{C.6}$$

$$A_1 = \arcsin\left(\frac{L}{2r}\right), \tag{C.7}$$

$$B_1 = \sqrt{1 - \frac{L^2}{4r^2}}, \tag{C.8}$$

where:
D_y — the shell bending flexural rigidity of the corrugated wall sheet for circumferential bending,
L — the length of the arc between the two columns,
r — the silo radius,
f — the height of the arch.

References

[1] J.G. Teng, X. Lin, J.M. Rotter, X.L. Ding, Analysis of geometric imperfections in full-scale welded steel silos, Eng. Struct. 27 (2005) 938–950.
[2] Ö. Zeybek, M. Seçer, A design approach for the ring girder in elevated steel silos, Thin-Walled Struct. 157 (2020) 10700.
[3] A.M. Mehretehran, S. Maleki, Axial buckling of imperfect cylindrical steel silos with isotropic walls under stored solids loads: FE analyses versus Eurocode provisions, Eng. Fail. Anal. 137 (2022) 106282.
[4] H. Jing, H. Chen, J. Yang, P. Li, Shaking table tests on a small-scale steel cylindrical silo model in different filling conditions, Structures 37 (2022) 698–708.
[5] C.L. Brown, J. Nielsen, Silos - fundamentals of theory, behaviour and design, E and FN Spon, 1998.
[6] N. Fayed, L. Otten, Handbook of Powder Science and Technology, Chapmann and Hall, 1984.
[7] J. Rotter, Guide for the Economic Design of Circular Metal Silos, Spon Press, 2001.
[8] S.S. Safarian, E.C. Harris, Design and Construction of Silos and Bunkers, Van Nostrand Reinhold Company, 1985.
[9] J. Tejchman, in: W. Wu, R.I. Borja (Eds.), Confined Granular Flow in Silos-Experiments and Numerical Investigations, Springer, Berlin-Heidelberg, 2013.
[10] M. Wójcik, J. Tejchman, Modelling of shear localization during confined granular flow in silos within non-local hypoplasticity, Powder Technol. 192 (3) (2009) 298–310.
[11] EN 1991-4. Eurocode 1: Actions on structures. Part 4: Silos and tanks: CEN, 2006.
[12] EN 1993-4-1. Eurocode 3: Design of steel structures. Part 4-1: Silos. Brussels: CEN, 2007.
[13] EN 1993-4-1:2007+A1:2017, Eurocode 3. Design of steel structures. Silos.
[14] P. Iwicki, K. Rejowski, J. Tejchman, Buckling of simplified models of silo with corrugated walls and vertical stiffeners, in: Shell Structures: Theory and Applications, Vol. 4, CRC Press/Balkema, London, 2018, pp. 235–238.
[15] P. Iwicki, K. Rejowski, J. Tejchman, Determination of buckling strength of silos composed of corrugated walls and thin-walled columns using simplified wall segment models, Thin-Walled Struct. 135 (2019) 414–436.
[16] P. Iwicki, K. Rejowski, J. Tejchman, Simplified numerical model for global stability of corrugated silos with vertical stiffeners, J. Construct. Steel Res. 138 (2017) 93–116.
[17] P. Iwicki, J. Tejchman, Stability of cylindrical steel silos composed of corrugated sheets and columns based on FE analyses versus Eurocode 3 approach, Eng. Fail. Anal. 57 (2015) 444–469.
[18] P. Iwicki, M. Sondej, J. Tejchman, Application of linear buckling sensitivity analysis to economic design of cylindrical steel silos composed of corrugated sheets and columns, Eng. Fail. Anal. 70 (2016) 105–121.
[19] P. Iwicki, M. Wójcik, J. Tejchman, Failure of cylindrical steel silos composed of corrugated sheets and columns and repair methods using a sensitivity analysis, Eng. Fail. Anal. 18 (8) (2011) 2064–2083.
[20] M. Sondej, P. Iwicki, J. Tejchman, M. Wójcik, Critical assessment of Eurocode approach to stability of metal cylindrical silos with corrugated walls and vertical stiffeners, Thin-Walled Struct. 95 (2015) 335–346.
[21] M. Sondej, P. Iwicki, M. Wójcik, J. Tejchman, Stability analyses of a cylindrical steel silo with corrugated sheets and columns, Steel Compos. Struct. 20 (1) (2016) 147–166.
[22] M. Wójcik, P. Iwicki, J. Tejchman, 3D buckling analysis of a cylindrical metal bin composed of corrugated sheets strengthened by vertical stiffeners, Thin-Walled Struct. 49 (8) (2011) 947–963.
[23] E. Hotała, L. Skotny, M. Kuśnierek, J. Boniecka, Experimental investigations on the resistance of vertical stiffeners of steel silos shells made of corrugated sheets, in: XIII International Conference on Metal Structures, CRC Press, Zielona Góra, 2016, pp. 499–506.
[24] K. Rejowski, P. Iwicki, Buckling analysis of cold formed silo column, Mech. Mech. Eng. 20 (2) (2016) 109–120.
[25] K. Rejowski, P. Iwicki, Simplified stability analysis of steel cylindrical silos with corrugated walls and vertical columns, in: Gizejowski, et al. (Eds.), Recent Progress in Steel and Composite Structures, Taylor & Francis Group, London, 2016, pp. 525–532.
[26] T. Ghanbari-Ghazijahani, H. Jiao, D. Holloway, Longitudinally stiffened corrugated cylindrical shells under uniform external pressure, J. Constr. Steel Res. 110 (2015) 191–199.
[27] T. Ghanbari-Ghazijahani, Dizaji H.S., J. Nozohor, T. Zirakian, Experiments on corrugated thin cylindrical shells under uniform external pressure, Ocean Eng. 106 (2015) 68–76.
[28] M. Wójcik, M. Sondej, K. Rejowski, J. Tejchman, Full-scale experiments on wheat flow in steel silo composed of corrugated walls and columns, Powder Technol. 311 (2017) 537–555.
[29] EN 1993-1-1: Eurocode 3: Design of steel. Part 1-1: General rules and rules for buildings (2004/18/EC).
[30] N. Kuczyńska, M. Wójcik, J. Tejchman, Effect of bulk solid on strength of cylindrical corrugated silos during filling, J. Construct. Steel Res. 115 (2015) 1–17.
[31] M. Wójcik, J. Tejchman, Simulation of buckling process of cylindrical metal silos with flat sheets containing bulk solids, Thin-Walled Struct. 93 (2015) 122–136.
[32] Dassault systèmes SIMULIA, in: Abaqus 2019, Documentations, 2019.
[33] P. Iwicki, J. Tejchman, J. Chróścielewski, Dynamic FE simulations of buckling process in thin-walled cylindrical metal silos, Thin-Walled Struct. 84 (2014) 344–359.
[34] J. Tejchman, J. Górski, Computations of size effects in granular bodies within micro-polar hypoplasticity during plane strain compression, Int. J. Solids Struct. 45 (6) (2008) 1546–1569.